Three-dimensional atom localization from spatial interference in a double two-level atomic system

Zhonghu Zhu,[1] Wen-Xing Yang,[1,2,*] Xiao-Tao Xie,[3] Shasha Liu,[1] Shaopeng Liu,[1] and Ray-Kuang Lee[2]
[1]*Department of Physics, Southeast University, Nanjing 210096, China*
[2]*Institute of Photonics Technologies, National Tsing-Hua University, Hsinchu 300, Taiwan*
[3]*School of Physics and Information Technology, Shanxi Normal University, Xi'an 710062, China*
(Received 9 October 2015; revised manuscript received 13 June 2016; published 13 July 2016)

We propose a efficient scheme for high-precision three-dimensional (3D) atom localization via spatial interference in a generic double two-level atomic system driven by a weak probe field and three mutually perpendicular standing-wave fields. Because the spatial interference originates from the position-dependent atom-field interaction, the position information of the atom can be obtained by the measurement of the atom population. We find that the precision of 3D atom localization in volumes depends sensitively on the frequency detuning and the phase shifts associated with the standing-wave fields. Interestingly enough, we show that adjusting the frequency detuning and phase shifts can lead to a redistribution of the atoms and a significant change in the visibility of the interference pattern. As a result, the atom can be localized in volumes that are substantially smaller than a cubic optical wavelength.

DOI: 10.1103/PhysRevA.94.013826

I. INTRODUCTION

The precision position measurement on an atomic scale is a longstanding issue and has attracted considerable attention because of its potential wide applications in laser cooling and trapping of neutral atoms [1,2], atom nanolithography [3,4], Bose–Einstein condensation [5–7], the measurement of the center-of-mass wave function of moving atoms [8], coherent patterning of matter waves [9], and so on. Usually, the spatial resolution cannot be better than the length scale given by the wavelength of the applied light beam due to that the diffractive scattering that takes place when a beam of atoms interacts with the periodic structure of light [10]. Note that there are some different methods for going beyond this limit for atom localization, such as the measurement of the atomic resonance frequency [11–13], the phase shift of the standing-wave field [14–16], and the atomic dipole [17].

On the other hand, several theoretical schemes have been proposed to obtain position information of moving atoms based on the atomic coherence and quantum interference effect. In these schemes, standing-wave driving fields have been used to encode position information into an intensity pattern via the position-dependent Rabi frequency. Considerable progress has been made in establishing the precision position of atoms, such as the quadrature phases of light fields interacting with the atom [18], long-lived electronic states [19,20], resonance fluorescence [21–23], absorption of light [24], and combinations thereof [25]. Subsequently, many efforts have been made to improve the accuracy of measurement. In this regard, we note that several proposals based on the atomic coherence and quantum interference effect have been made via different measurement schemes, such as amplitude- and phase-dependent emission [26] and absorption spectra [27,28], coherent population trapping (CPT) [29], dark resonances [30], and multiple simultaneous measurements [31–34].

In recent years, two-dimensional (2D) atom localization by applying two orthogonal standing-wave fields has attracted considerable interest because of a better prospect of application and unique properties in contrast with the one-dimensional (1D) schemes mentioned above. Note that, in 2D atom localization, one can obtain mere subwavelength localization as well as spatial structuring of the atomic locations. For 2D atom localization, Ivanov and Rozhdestvensky [35] presented a scheme for 2D subwavelength localization in a four-level tripod system and found that the localization factors depend crucially on the atom-field coupling, which results in such spatial structures of population as spikes, craters, and waves. Another related 2D-atom-localization scheme has been proposed [36] by controlled spontaneous emission in a four-level atomic system with a closed loop. Afterwards, several high-precision and high-resolution 2D-atom-localization schemes have been reported [37–40] for different-configuration atomic systems.

A key question is whether subwavelength localization can also be achieved in the three-dimensional (3D) case. Possible applications of 3D atom localization may include high-precision position-dependent state-selective chemical reactions. More recently, several schemes have been put forward for 3D atom localization that use three mutually perpendicular standing-wave fields [41,42]. For instance, a scheme for 3D atom localization based on EIT was demonstrated in Ref. [41] by measuring the probe absorption in a five-level M-type atomic system. Afterwards, the different 3D periodic structures in 3D space were achieved by Ivanov and coworkers [42] via the measurement of the atomic-level population in a four-level tripod-type atomic system. The previous schemes for 3D atom localization [41,42] contend that the different localization patterns of atoms are situated in the eight subspaces (x,y,z), $(-x,y,z)$, $(x,-y,z)$, $(x,y,-z)$, $(-x,-y,z)$, $(x,-y,-z)$, $(-x,y,-z)$, and $(-x,-y,-z)$. Thus, it reminds us of another question: Can we localize the atom in one subspace with a greater probability of localizing the atom in 3D space than the previous schemes?

To further improve the precision of 3D atom localization and the probability of localizing the atom in a cubic optical wavelength, we propose a scheme for realizing high-precision 3D atom localization in a generic duplicated two-level atomic system by measuring the atomic-level population. By properly

*wenxingyang2@126.com

adjusting the system parameters, we can localize the atom in one subspace, and the probability of finding the atom in 3D space is increased by a factor of eight compared with the previous schemes [41,42]. Interestingly enough, we show that, in the weak driven situation, adjusting the phase shifts associated with the standing-wave fields leads to a redistribution of the atoms and a significant change of the visibility of the interference pattern so that the atom can be localized in volumes that are substantially smaller than a cubic optical wavelength.

II. THEORETICAL MODEL AND BASIC EQUATIONS

Let us consider a double two-level atomic system with two degenerate ground states $|1\rangle$ and $|2\rangle$ and two degenerate excited states $|3\rangle$ and $|4\rangle$, as shown in Fig. 1(a). The transitions between levels $|1\rangle$ and $|3\rangle$ (with transition frequency ω_{31}) and between levels $|2\rangle$ and $|4\rangle$ (with transition frequency ω_{42}) are coupled simultaneously by the relevant standing-wave field with position-dependent Rabi frequency $G_s(x,y,z)$. A degenerate σ-polarized probe field E_p (with angular frequency ω_p and Rabi frequency $2\Omega_p$) is applied to drive simultaneously the electric-dipole transitions between levels $|1\rangle$ and $|4\rangle$ (with transition frequency ω_{41}) and between levels $|2\rangle$ and $|3\rangle$ (with transition frequency ω_{32}). It is worth pointing out that $G_s(x,y,z)$ corresponds to the combination of three orthogonal standing-wave fields that drives simultaneously the transitions $|1\rangle \leftrightarrow |3\rangle$ and $|2\rangle \leftrightarrow |4\rangle$, i.e.,

$$G_s(x,y,z) = G_s(x) + G_s(y) + G_s(z), \tag{1}$$

where $G_s(x)$, $G_s(y)$, and $G_s(z)$ are also the combinations of two orthogonal standing-wave fields aligning along the corresponding x, y, and z directions, respectively, i.e.,

$$G_s(x) = \Omega_1[\sin(\kappa_1 x + \varphi) + \sin(\kappa_2 x)], \tag{2}$$

$$G_s(y) = \Omega_2[\sin(\kappa_3 y + \phi) + \sin(\kappa_4 y)], \tag{3}$$

$$G_s(z) = \Omega_3[\sin(\kappa_5 z + \eta) + \sin(\kappa_6 z)], \tag{4}$$

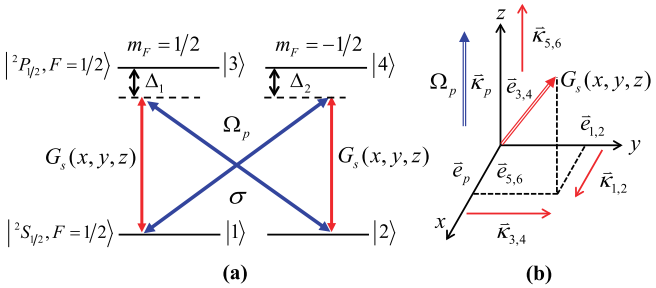

FIG. 1. (a) The energy-level diagram of a generic double two-level atomic system interacting with a weak probe field Ω_p and a combination of three mutually perpendicular standing-wave fields $G_s(x,y,z)$. Δ_1 and Δ_2 represent the relevant frequency detunings. Note that $\Delta_1 = \Delta_2 = \Delta$ in the present system. (b) Field configurations.

with $\kappa_i = 2\pi/\lambda_i$ ($i = 1$–6) being the wave vectors corresponding to wavelength λ_i of the relevant standing-wave fields. Here, for simplicity, we assume $\Omega_1 = \Omega_2 = \Omega_3 = \Omega_s$. The parameters φ, ϕ, and η are the phase shifts of the relevant standing-wave fields corresponding to wave vectors κ_1, κ_3, and κ_5, respectively. An atom moves along the z direction and passes through the intersecting region of the three mutually perpendicular standing-wave fields in 3D space. As a result, the interaction between the atom and the standing-wave fields is spatially dependent on the 3D space.

Such an atomic structure can be realized in cold ^{6}Li atoms [43] using the D_1-line with the transition $2\,^2S_{1/2} \rightarrow 2\,^2P_{1/2}$. The designated states can be chosen as follows: $|1\rangle = |2\,^2S_{1/2}, F = \frac{1}{2}, m_F = \frac{1}{2}\rangle$, $|2\rangle = |2\,^2S_{1/2}, F = \frac{1}{2}, m_F = -\frac{1}{2}\rangle$, $|3\rangle = |2\,^2P_{1/2}, F = \frac{1}{2}, m_F = \frac{1}{2}\rangle$, and $|4\rangle = |2\,^2P_{1/2}, F = \frac{1}{2}, m_F = -\frac{1}{2}\rangle$, respectively. According to the Wigner–Eckart theorem [44,45], the electric-dipole matrix element for the corresponding transition is proportional to the Clebsch–Gordan coefficient $\langle (J'I')F'm_{F'}|(JI)F1m_Fq\rangle$ [46], i.e.,

$$\langle (J'I')F'm_{F'}|\hat{\mu}(1,q)|(JI)Fm_F\rangle = \langle (J'I')F'||\hat{\mu}(1)||(JI)F\rangle \langle (J'I')F'm_{F'} \mid (JI)F1m_Fq\rangle. \tag{5}$$

In such case, the Clebsch–Gordan coefficient can be given by the 3-j symbol,

$$\langle (J'I')F'm_{F'} \mid (JI)F1m_Fq\rangle = (-1)^{F'-m_{F'}} \begin{pmatrix} J' & 1 & J \\ -m_{F'} & q & m_F \end{pmatrix}. \tag{6}$$

On the other hand, the proportionality factor is factorized into the reduced matrix element $\langle J'||\hat{\mu}(1)||J\rangle$ and the corresponding Wigner 6-j symbol can be given by

$$\langle (J'I')F'||\hat{\mu}(1)||(JI)F\rangle = \delta_{I'I}(-1)^{J'+I+F+1}\sqrt{(2F'+1)(2F+1)} \begin{Bmatrix} J' & I & F' \\ F & 1 & J \end{Bmatrix} \langle J'||\hat{\mu}(1)||J\rangle, \tag{7}$$

where the ^{6}Li D_1 line is defined by the total angular momentum $I = \frac{1}{2}$. Thus, the value of the D_1-line reduced matrix element is

$$\langle J' = 1/2||\hat{\mu}(1)||J = 1/2\rangle = -\sqrt{2}\mu_0 = -2.812 \times 10^{-29}\ \text{C.m.}, \tag{8}$$

where C.m. (i.e., Coulomb multiplied by metre) denotes SI units of electric dipole moment.

In addition, the decay rate via the Einstein A coefficient [47,48] can be given by

$$\frac{1}{\tau} = \frac{\omega^3}{3\pi\varepsilon_0\hbar c^3}\frac{1}{(2J+1)}|\langle J'||\hat{\mu}(1)||J\rangle|^2. \tag{9}$$

It is worth pointing out that in our present atomic system, the corresponding matrix elements of the dipole operator are given by

$$\hat{\mu}_{42} = \sqrt{\frac{1}{54}}\langle J = 1/2||\hat{\mu}(1)||J' = 1/2\rangle,$$
$$\hat{\mu}_{31} = -\sqrt{\frac{1}{54}}\langle J = 1/2||\hat{\mu}(1)||J' = 1/2\rangle,$$
$$\hat{\mu}_{32} = \sqrt{\frac{1}{27}}\langle J = 1/2||\hat{\mu}(1)||J' = 1/2\rangle,$$
$$\hat{\mu}_{41} = -\sqrt{\frac{1}{27}}\langle J = 1/2||\hat{\mu}(1)||J' = 1/2\rangle. \quad (10)$$

At the same time, the atomic dipole operator is the sum of atomic raising $\mu^{\uparrow}$ and lowering $\mu^{\downarrow}$ operators, whose components are [49]

$$\mu_x^{\downarrow} = \mu(|2\rangle\langle 3| - |1\rangle\langle 4|)\hat{x}, \quad (11)$$
$$\mu_y^{\downarrow} = i\mu(|2\rangle\langle 3| + |1\rangle\langle 4|)\hat{y}, \quad (12)$$
$$\mu_z^{\downarrow} = \mu(|2\rangle\langle 4| - |1\rangle\langle 3|)\hat{z}, \quad (13)$$

where $\mu_k^{\downarrow}$ is the k component of the atomic dipole, μ is the dipole matrix element, and $\hat{x}$, $\hat{y}$, and $\hat{z}$ are the usual Cartesian unit vectors.

Here we assume that the center-of-mass position distribution of the atom along the directions of the standing-wave fields is nearly constant and we can ignore the kinetic energy of the atom in the Hamiltonian by applying the Raman–Nath approximation [44]. By choosing $H_0 = (\omega_s - \omega_p)|2\rangle\langle 2| + \omega_s|3\rangle\langle 3| + \omega_p|4\rangle\langle 4|$ and taking level $|1\rangle$ as the energy origin, under the electric dipole approximation (EDA) and the rotating-wave approximation (RWA), the interaction Hamiltonian of the present atomic system is given by ($\hbar = 1$):

$$H_{\rm int} = \Delta|3\rangle\langle 3| + \Delta|4\rangle\langle 4| - [\Omega_p(|3\rangle\langle 2| - |4\rangle\langle 1|) + G_s(x,y,z)(|4\rangle\langle 2| - |3\rangle\langle 1|) + \text{H.c.}], \quad (14)$$

where the symbol H.c. represents the Hermitian conjugate. $\Delta_1 = \omega_{31} - \omega_s = \omega_{32} - \omega_p$ and $\Delta_2 = \omega_{41} - \omega_p = \omega_{42} - \omega_s$ represent the relevant frequency detunings. It is obvious that $\Delta_1 = \Delta_2 = \Delta$ in the present system. $\Omega_p = \mu_{32}E_p/(2\hbar) = -\mu_{41}E_p/(2\hbar)$ and $G_s(x,y,z) = \Omega_s[\sin(\kappa_1 x + \varphi) + \sin(\kappa_2 x) + \sin(\kappa_3 y + \phi) + \sin(\kappa_4 y) + \sin(\kappa_5 z + \eta) + \sin(\kappa_6 z)]$, with $\Omega_s = \mu_{42}E_s/(2\hbar) = -\mu_{31}E_s/(2\hbar)$ being the half Rabi frequencies of the probe field and the standing-wave fields for the relevant driven transitions, respectively, and where $\mu_{ij} = \vec{\mu}_{ij} \cdot \vec{e}_L$ $(i,j = 1\text{–}4)$ denotes the dipole matrix moment for the relevant optical transition from level $|i\rangle$ to level $|j\rangle$ with $\vec{e}_L$ denoting the unit polarization vector of the corresponding laser field.

The dynamics of this system can be described by using the density-matrix approach as

$$\dot{\rho} = -\frac{i}{\hbar}[H_{\rm int}, \rho] + L[\rho(t)], \quad (15)$$

where the Liouvillian matrix $L[\rho(t)]$ denoting the relaxation by spontaneous decay can be given by

$$L[\rho(t)] = \begin{pmatrix} (\Gamma_{31}\rho_{33} + \Gamma_{41}\rho_{44}) & 0 & -\frac{\Gamma_{13}+\Gamma_{23}}{2}\rho_{13} & -\frac{\Gamma_{14}+\Gamma_{24}}{2}\rho_{14} \\ 0 & (\Gamma_{32}\rho_{33} + \Gamma_{42}\rho_{44}) & -\frac{\Gamma_{23}+\Gamma_{13}}{2}\rho_{23} & -\frac{\Gamma_{24}+\Gamma_{14}}{2}\rho_{24} \\ -\frac{\Gamma_{31}+\Gamma_{32}}{2}\rho_{31} & -\frac{\Gamma_{32}+\Gamma_{31}}{2}\rho_{32} & -(\Gamma_{31}+\Gamma_{32})\rho_{33} & 0 \\ -\frac{\Gamma_{41}+\Gamma_{42}}{2}\rho_{41} & -\frac{\Gamma_{42}+\Gamma_{41}}{2}\rho_{42} & 0 & -(\Gamma_{41}+\Gamma_{42})\rho_{44} \end{pmatrix}, \quad (16)$$

where Γ_{ij} $(i,j = 1\text{–}4)$ denotes the coherent decay rate from level $|i\rangle$ to level $|j\rangle$. It is worth pointing out that $\Gamma_{31} = \Gamma_{13} = \Gamma_{42} = \Gamma_{24} = \frac{1}{54}\Gamma$ and $\Gamma_{41} = \Gamma_{14} = \Gamma_{32} = \Gamma_{23} = \frac{1}{27}\Gamma$, where $\Gamma = \frac{\omega^3}{6\pi\varepsilon_0\hbar c^3}|\langle J = 1/2||\hat{\mu}(1)||J' = 1/2\rangle|^2$ with $|\langle J = 1/2||\hat{\mu}(1)||J' = 1/2\rangle|^2$ denoting the D_1-line reduced matrix element for ^{6}Li atoms.

By substituting the interaction Hamiltonian given by Eq. (14) into Eq. (15), the coupled equations of motion for the corresponding density-matrix elements can be given as

$$\dot{\rho}_{22} = (\Gamma_{32}\rho_{33} + \Gamma_{42}\rho_{44}) + i\Omega_p^*\rho_{32} - i\Omega_p\rho_{23} + iG_s^*(x,y,z)\rho_{42} - iG_s(x,y,z)\rho_{24}, \quad (17)$$
$$\dot{\rho}_{33} = -(\Gamma_{31} + \Gamma_{32})\rho_{33} - i\Omega_p^*\rho_{32} + i\Omega_p\rho_{23} + iG_s^*(x,y,z)\rho_{31} - iG_s(x,y,z)\rho_{13}, \quad (18)$$
$$\dot{\rho}_{44} = -(\Gamma_{41} + \Gamma_{42})\rho_{44} + i\Omega_p^*\rho_{41} - i\Omega_p\rho_{14} - iG_s^*(x,y,z)\rho_{42} + iG_s(x,y,z)\rho_{24}, \quad (19)$$
$$\dot{\rho}_{21} = i\Omega_p^*\rho_{31} + i\Omega_p\rho_{24} + iG_s^*(x,y,z)\rho_{41} + iG_s(x,y,z)\rho_{23}, \quad (20)$$
$$\dot{\rho}_{31} = -\left(\frac{\Gamma_{31} + \Gamma_{32}}{2} + i\Delta\right)\rho_{31} + i\Omega_p\rho_{21} + i\Omega_p\rho_{34} + iG_s(x,y,z)(\rho_{33} - \rho_{11}), \quad (21)$$
$$\dot{\rho}_{41} = -\left(\frac{\Gamma_{41} + \Gamma_{42}}{2} + i\Delta\right)\rho_{41} + i\Omega_p(\rho_{44} - \rho_{11}) + iG_s(x,y,z)\rho_{21} + iG_s(x,y,z)\rho_{43}, \quad (22)$$
$$\dot{\rho}_{32} = -\left(\frac{\Gamma_{32} + \Gamma_{31}}{2} + i\Delta\right)\rho_{32} + i\Omega_p(\rho_{22} - \rho_{33}) - iG_s(x,y,z)\rho_{12} - iG_s(x,y,z)\rho_{34}, \quad (23)$$
$$\dot{\rho}_{42} = -\left(\frac{\Gamma_{42} + \Gamma_{41}}{2} + i\Delta\right)\rho_{42} - i\Omega_p\rho_{12} - i\Omega_p\rho_{43} + iG_s(x,y,z)(\rho_{22} - \rho_{44}), \quad (24)$$

$$\dot{\rho}_{43} = -i\Omega_p\rho_{13} - i\Omega_p^*\rho_{42} + iG_s(x,y,z)\rho_{23} + iG_s^*(x,y,z)\rho_{41}, \tag{25}$$

together with $\rho_{ij} = \rho_{ji}^*$ $(i,j = 1\text{–}4)$ and $\sum_{j=1}^4 \rho_{jj} = 1$.

We define $n_e = \rho_{33} + \rho_{44}$ as the excited population, and the coherent terms $\rho_\pi = \rho_{42} - \rho_{31}$, $\rho_\sigma = \rho_{32} - \rho_{41}$ are responsible for the combination of three orthogonal standing-wave fields $G_s(x,y,z)$ and the σ-polarized field, respectively. Note that the measurement of the excited population (i.e., $\rho_{33} + \rho_{44}$) can directly obtain the position information of the atom when the atom passes through the standing-wave fields in 3D space. Under the weak-field approximation (i.e., $\Omega_p \ll \Omega_1, \Omega_2, \Omega_3$) and considering the normalization condition of the present system (i.e., $\sum_{j=1}^4 \rho_{jj} = 1$), the exact steady-state results by using professional computing software (i.e., Wolfram *Mathematica*) can be given by

$$n_e = \frac{4[|G_s(x,y,z)|^2 - |\Omega_p|^2]^2}{(4\Delta^2 + D^2)[|G_s(x,y,z)|^2 + |\Omega_p|^2] + 8[|G_s(x,y,z)|^2 - |\Omega_p|^2]^2}, \tag{26}$$

$$\rho_\sigma = -\frac{2(2\Delta + iD)[|G_s(x,y,z)|^2 - |\Omega_p|^2]\Omega_p}{(4\Delta^2 + D^2)[|G_s(x,y,z)|^2 + |\Omega_p|^2] + 8[|G_s(x,y,z)|^2 - |\Omega_p|^2]^2}, \tag{27}$$

$$\rho_\pi = \frac{2(2\Delta + iD)[|G_s(x,y,z)|^2 - |\Omega_p|^2]G_s(x,y,z)}{(4\Delta^2 + D^2)[|G_s(x,y,z)|^2 + |\Omega_p|^2] + 8[|G_s(x,y,z)|^2 - |\Omega_p|^2]^2}, \tag{28}$$

where $D = \Gamma_{32} + \Gamma_{42}$.

Equation (26) reflects the conditional position probability distribution of the atom in 3D space [42]. Therefore, the 3D atom localization behavior near point (x_0, y_0, z_0) (i.e., $x_0 = 2l\frac{\lambda}{4}$, $y_0 = 2m\frac{\lambda}{4}$, $z_0 = 2n\frac{\lambda}{4}$ with l as well as m and n being integers) including the increase of the detecting probability and improvement of the localization precision can be controlled by adjusting the system parameters.

III. NUMERICAL RESULTS AND DISCUSSIONS

In this section, we investigate the conditional position probability distribution of the atom in 3D space via a few numerical calculations based on the excited population $(\rho_{33} + \rho_{44})$ in Eq. (26) and then achieve high-precision 3D atom localization by measuring the population of the levels $|3\rangle$ and $|4\rangle$. To give a clear illustration, we select $\Gamma = 3.6898 \times 10^7\ \mathrm{s}^{-1}$, $\Omega_s = 0.75\Gamma$, $\Omega_p = 0.01\Gamma$, and all the parameters used in the following numerical calculations are in units of Γ. Subsequently, we present a few numerical results for 3D atom localization with different values of the relevant parameters to illustrate that high-precision 3D atom localization can be achieved in the present double two-level atomic system.

First of all, we investigate the influence of the frequency detuning of the relevant optical fields Δ on 3D atom localization near point (x_0, y_0, z_0) without considering the phase shifts of the standing-wave fields (i.e., $\varphi = \phi = \eta = 0$). From Fig. 2, one can find that the spatial distribution as well as the precision of 3D atom localization are dependent on the frequency detuning of the relevant optical fields. In the case of $\Delta = 2.15\Gamma$ [see Fig. 2(a) (a)], two ellipsoidal structures with the same size are situated in the two subspaces $(-x,-y,-z)$ and (x,y,z), respectively. When the frequency detuning of the relevant optical fields Δ increases to 3.15Γ with keeping all other parameters fixed, the localization pattern of atoms in the two subspaces is still ellipsoid like but with the smaller sizes [see Fig. 2(b)]. Direct comparison of Figs. 2(a) and 2(b) implies that the precision of 3D atom localization can be significantly improved when the frequency detuning of the relevant optical fields Δ increases. Thus, high-precision of 3D atom localization is indeed achieved via adjusting the frequency detuning of the relevant optical fields.

The above interesting localization phenomena as shown in Fig. 2 originates from the far-field phase-dependent spatial interference induced by the optical fields. For calculating the far-field phase-dependent spatial interference pattern, we assume that the atoms interacting with the optical fields are identical and independent of each other. Let us consider the observing screen being placed in the far field (large y) and oriented in the x-z plane. We label a point on the screen by (τ_1, τ_2), where τ_i $(i = 1,2)$ is the light travel time from the ith atom to the observation point. Thus, the intensity of the light at this point is given by [50–52]

$$I(\tau_1,\tau_2) \propto \langle E_x^\uparrow E_x^\downarrow + E_z^\uparrow E_z^\downarrow \rangle, \tag{29}$$

where

$$E_k^\uparrow(t;\tau_1,\tau_2) \propto e^{-i\omega(t-\tau_1)}u_k^\uparrow + e^{-i\omega(t-\tau_2)}U_k^\uparrow, \tag{30}$$

for $k \in \{x,z\}$, u and U are the atomic dipoles of the first and second atoms, respectively, and ω is the angular frequency of the laser light. Since we assumed that the atoms are independent and identical, the intensity of the interference pattern when all light is detected is given by

$$\begin{aligned} I(\tau_1,\tau_2) \propto\ & \langle u_x^\uparrow u_x^\downarrow + U_x^\uparrow U_x^\downarrow + u_z^\uparrow u_z^\downarrow + U_z^\uparrow U_z^\downarrow \rangle \\ & + \langle u_x^\uparrow U_x^\downarrow \rangle e^{i\omega(\tau_1-\tau_2)} + \langle u_x^\downarrow U_x^\uparrow \rangle e^{-i\omega(\tau_1-\tau_2)} \\ & + \langle u_z^\uparrow U_z^\downarrow \rangle e^{i\omega(\tau_1-\tau_2)} + \langle u_z^\downarrow U_z^\uparrow \rangle e^{-i\omega(\tau_1-\tau_2)}. \end{aligned} \tag{31}$$

The components in Eq. (31) in the steady state can be given by

$$\begin{aligned} \langle u_x^\uparrow u_x^\downarrow \rangle_{ss} &= \langle U_x^\uparrow U_x^\downarrow \rangle_{ss} \\ &\propto \mu^2 \langle (|3\rangle\langle 2| - |4\rangle\langle 1|)(|2\rangle\langle 3| - |1\rangle\langle 4|) \rangle_{ss} \\ &= \mu^2 \langle |3\rangle\langle 3| + |4\rangle\langle 4| \rangle_{ss} \\ &= \mu^2 n_e, \end{aligned} \tag{32}$$

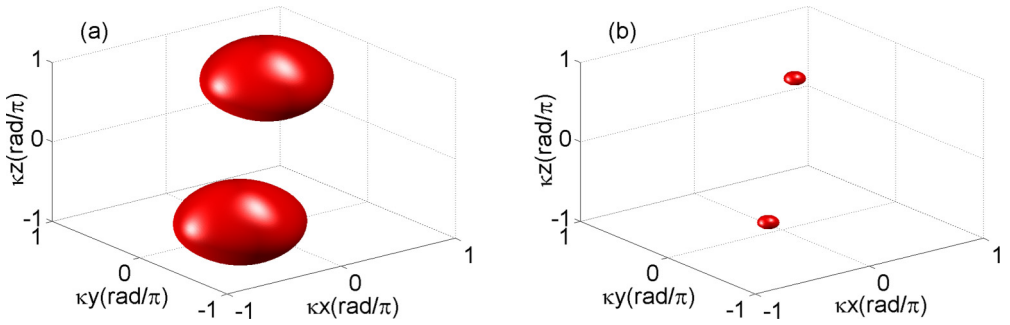

FIG. 2. The excited population $n_e = 0.4$ as functions of $(\kappa x,\kappa y,\kappa z)$ for different frequency detunings Δ with the units of the wave vector κ being rad/nm. (a) $\Delta = 2.15\Gamma$; (b) $\Delta = 3.15\Gamma$. The other values of the parameters are $\Gamma = 3.6898 \times 10^7\ \mathrm{s}^{-1}$, $\Gamma_{32} = \frac{1}{27}\Gamma$, $\Gamma_{42} = \frac{1}{54}\Gamma$, $\Omega_s = 0.75\Gamma$, $\Omega_p = 0.01\Gamma$, $\kappa_1 = \kappa_3 = \kappa_5 = \kappa$, $\kappa_2 = \kappa_4 = \kappa_6 = \kappa$, and $\varphi = \phi = \eta = 0$.

and similarly

$$\langle u_z^{\uparrow} u_z^{\downarrow}\rangle_{ss} = \langle U_z^{\uparrow} U_z^{\downarrow}\rangle_{ss} = \mu^2 n_e, \tag{33}$$

$$\langle u_x^{\uparrow} U_x^{\downarrow}\rangle_{ss} = \langle u_x^{\uparrow} U_x^{\uparrow}\rangle_{ss}^{*} \propto \mu^2 \langle u_x^{\uparrow}\rangle_{ss} \langle U_x^{\downarrow}\rangle_{ss} = \mu^2 \rho_\sigma \rho_\sigma^{*}, \tag{34}$$

$$\langle u_z^{\uparrow} U_z^{\downarrow}\rangle_{ss} = \langle u_z^{\uparrow} U_z^{\uparrow}\rangle_{ss}^{*} \propto \mu^2 \langle u_z^{\uparrow}\rangle_{ss} \langle U_z^{\downarrow}\rangle_{ss} = \mu^2 \rho_\pi \rho_\pi^{*}. \tag{35}$$

Thus, in our duplicated two-level atomic system, the visibility of the interference pattern, which is defined as $V = (I_{\max} - I_{\min})/(I_{\max} - I_{\min})$, can be calculated by using the steady-state solutions [Eqs. (26)–(28)]:

$$V = \frac{1}{2n_e}(\rho_\pi \rho_\pi^{*} + \rho_\sigma \rho_\sigma^{*}) = \frac{(4\Delta^2 + D^2)[|G_s(x,y,z)|^2 + |\Omega_p|^2]}{2(4\Delta^2 + D^2)[|G_s(x,y,z)|^2 + |\Omega_p|^2] + 16[|G_s(x,y,z)|^2 - |\Omega_p|^2]^2}, \tag{36}$$

where $D = \Gamma_{32} + \Gamma_{42}$.

According to Eq. (36), we plot the visibility V as functions of $(\Delta,\kappa z)$ at the expected position [i.e., $(\kappa x,\kappa y) = (\pm 0.55\pi,\pm 0.55\pi)$], as shown in Fig. 3. Figure 3(a) shows that the visibility is mainly covered in the positive direction of the Oz axis when $(\kappa x,\kappa y) = (0.55\pi,0.55\pi)$ and the values of other parameters are the same as in Fig. 2. When κx and κy are tuned to $(\kappa x,\kappa y) = (-0.55\pi,-0.55\pi)$ with all other parameters the same as in Fig. 3(a), the visibility is mainly situated in the negative direction of the Oz axis, as shown in Fig. 3(b). From Figs. 3(a) and 3(b), one can find that, upon increasing Δ from 2.15Γ to 3.15Γ, the values of visibility increase progressively when κz remains fixed [see points A and B labeled in Figs. 3(a) and 3(b)]. That is, the increase of the spatial interference will lead to the size of the 3D localization structure becoming smaller, which gives the physical reason for the sizes of 3D localization structures being changed in going from Fig. 2(a) to Fig. 2(b).

It is desirable to obtain the position of the atom when the atom passes through the standing-wave fields. The present scheme for 3D atom localization is based on the fact that the conditional probability distribution of the atom carries the information about the atomic position. Therefore, one can extract the localization information by means of a similar measurement scheme for 1D and 2D atom localization reported in Refs. [23,39]. We noticed that the previous scheme [39] for 2D atom localization had shown that the phase shifts played an important role in the spatial measurement of the atom in two dimensions and a single atom localization peak could be observed when one chose slightly different wavelengths of the standing-wave fields. Here we will investigate the influences of the phase shifts (φ,ϕ,η) of three orthogonal standing-wave fields on the behavior of 3D atom localization. In Fig. 4, we plot the excited population $n_e = 0.4$ as functions of $(\kappa x,\kappa y,\kappa z)$ in dependence on the phase shift (φ,ϕ,η) of three perpendicular standing-wave fields with slightly different wavelengths. In the condition of $\kappa_1 = \kappa_3 = \kappa_5 = \kappa$ and $\varphi = \phi = \eta = 0$, it can be found from Fig. 4(a) that two ellipsoidal structures with the same size are situated in two subspaces $(-x,-y,-z)$ and (x,y,z), respectively. Such a result is the same as in Fig. 2(a). When the phase shifts φ and ϕ are both equal to $\pi/2$, and the wave vectors κ_1 and κ_3 are both equal to 0.85κ, the localization patterns of the atoms in Fig. 4(b) are still ellipsoid like, where the smaller one is situated in subspace $(-x,-y,-z)$ while the bigger one is situated in subspace (x,y,z). Different from Fig. 4(a), the equal-probability-distribution situation has been destroyed when the phase shifts φ and ϕ of the corresponding standing-wave fields are nonzero. In such a case, the phase-dependent spatial-interference effect induced by the standing-wave fields and the probe field shows up. As a result, the corresponding atom localization precision in subspace $(-x,-y,-z)$ is significantly improved compared with Fig. 4(a). More interestingly, for the case that $(\kappa_1,\kappa_3,\kappa_5) = (0.85\kappa,0.85\kappa,0.85\kappa)$ and $(\varphi,\phi,\eta) = (\pi/2,\pi/2,\pi/2)$, the ellipsoidal shell in subspace $(-x,-y,-z)$ disappears, and the size of ellipsoidal shell localized in subspace (x,y,z) becomes smaller, as shown in Fig. 4(c), in which the probability of finding the atom in 3D space is indeed increased by a factor of two compared with Fig. 4(b). The above results demonstrate that the behavior of 3D atom localization is sensitive to

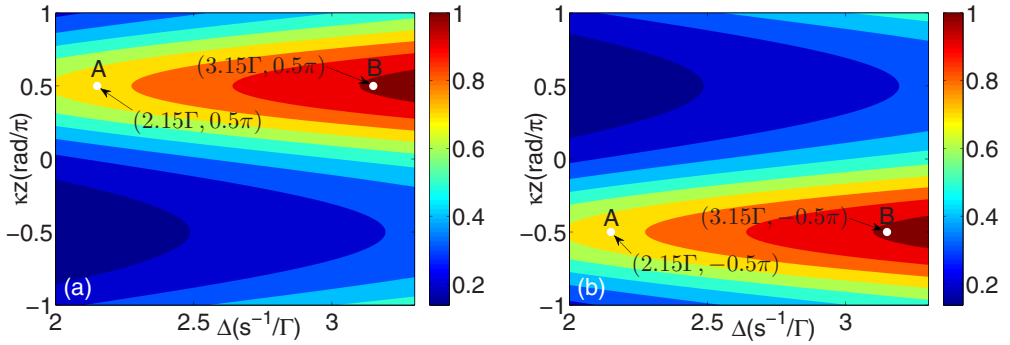

FIG. 3. The visibility V as functions of $(\Delta,\kappa z)$ for different situations with the units of the wave vector κ being rad/nm. (a) $(\kappa x,\kappa y) = (0.55\pi,0.55\pi)$; (b) $(\kappa x,\kappa y) = (-0.55\pi,-0.55\pi)$. The other values of the parameters are $\Gamma = 3.6898 \times 10^7\ \mathrm{s}^{-1}$, $\Gamma_{32} = \frac{1}{27}\Gamma$, $\Gamma_{42} = \frac{1}{54}\Gamma$, $\Omega_s = 0.75\Gamma$, $\Omega_p = 0.01\Gamma$, $\kappa_1 = \kappa_3 = \kappa_5 = \kappa$, $\kappa_2 = \kappa_4 = \kappa_6 = \kappa$, and $\varphi = \phi = \eta = 0$.

the phase shift (φ,ϕ,η) associated with three orthogonal standing-wave fields having slightly different wavelengths and also demonstrate the sensitive phase-related property of double two-level atomic systems.

For exploring the physical reason for the improvement of the 3D-atom-localization precision as shown in Figs. 4(a) and 4(b), we draw plots of the visibility V as functions of $(\varphi = \phi,\kappa_1 = \kappa_3)$ at certain (x,y,z) according to Eq. (36) [see Figs. 5(a) and 5(b)]. By direct comparison in Figs. 4(a) and 4(b), we obtain that the 3D-localization precision in subspace (x,y,z) is almost not changed while the 3D-localization precision in subspace $(-x,-y,-z)$ is significantly enhanced. From Fig. 5(a), one can find that, when (x,y,z) are tuned to $(x,y,z) = (0.5,0.5,0.5)$, keeping all other parameters the same as in Figs. 4(a) and 4(b), the visibilities of the points A and B labeled in Fig. 5(a) are almost equal, which explains the reasons for the 3D-localization precision in subspace (x,y,z) remaining almost unchanged from Fig. 4(a) to Fig. 4(b). For the case that $(x,y,z) = (-0.3,-0.3,-0.35)$, Fig. 5(b) shows that the visibility enhances significantly as the phase shifts φ and ϕ are simultaneously changed from 0 to $\pi/2$ with the wave vectors κ_1 and κ_3 remaining fixed [see points A and B labeled in Fig. 5(b)]. Such a result gives the physical reason for the sizes of the 3D localization structures in subspace $(-x,-y,-z)$ being changed from Fig. 4(a) to Fig. 4(b). Furthermore, for fully understanding the influence of the phase-dependent spatial interference on the 3D localization precision, we plot the visibility V versus the wave vector κ_5 and the phase shift η at expected position [i.e., $(x,y,z) = (0.5,0.5,0.5)$ and $(x,y,z) = (-0.3,-0.3,-0.35)$] as shown in Figs. 5(c) and 5(d). From Fig. 5(c), we can find that the values of the visibility in subspace (x,y,z) remain almost unchanged with (η,κ_5) being changed from $(\eta,\kappa_5) = (0,\kappa)$ to $(\eta,\kappa_5) = (\pi/2,0.85\kappa)$ [see points A and B labeled in Fig. 5(c)]. That is, if we only adjust the values of the wave vector κ_5 and the phase shift η but with keep all other parameters fixed, the atom will still be localized in subspace (x,y,z), and the precision of the 3D localization will be almost not changed. Based on the distribution of the visibility shown in Fig. 5(c), the results about the population distribution in subspace (x,y,z) shown in Figs. 4(b) and 4(c) can be also understood clearly. More interestingly, when the expected position is tuned to $(x,y,z) = (-0.3,-0.3,-0.35)$ with keeping all other parameters being same as Fig. 5(c), the atom will be localized in subspace $(-x,-y,-z)$, and it can be found from Fig. 5(d) that the distribution of the visibility is similar to Fig. 5(b). In such case, the visibility reaches its maximum value when (η,κ_5) is tuned to $(\eta,\kappa_5) = (\pi/2,0.85\kappa)$ [see point B labeled in Fig. 5(d)]. Thus, it is reasonable to achieve the high-precision 3D atom localization in Fig. 4(c).

To obtain a better understanding of how the excited population n_e modifies the 3D atom localization behavior, we draw plots of 3D conditional position probability distribution versus the normalized position $(\kappa x,\kappa y,\kappa z)$ for three different values of the excited population, as shown in Fig. 6. Figure 6 shows that the precision of the 3D atom localization depends sensitively on the excited population n_e. When n_e is equal to 0.355 with keeping all other parameters being same as

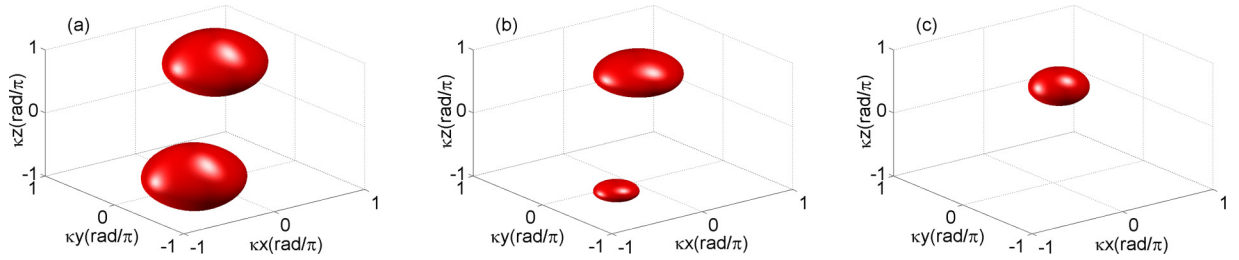

FIG. 4. The excited population $n_e = 0.4$ as functions of $(\kappa x,\kappa y,\kappa z)$ in dependence on the phase shifts (φ,ϕ,η) of the standing-wave fields with slightly different wavelengths. (a) $(\kappa_1,\kappa_3,\kappa_5) = (\kappa,\kappa,\kappa)$, $(\varphi,\phi,\eta) = (0,0,0)$; (b) $(\kappa_1,\kappa_3,\kappa_5) = (0.85\kappa,0.85\kappa,\kappa)$, $(\varphi,\phi,\eta) = (\pi/2,\pi/2,0)$; (c) $(\kappa_1,\kappa_3,\kappa_5) = (0.85\kappa,0.85\kappa,0.85\kappa)$, $(\varphi,\phi,\eta) = (\pi/2,\pi/2,\pi/2)$. The wave vector κ has units of rad/nm. The other values of the parameters are $\Gamma = 3.6898 \times 10^7\ \mathrm{s}^{-1}$, $\Gamma_{32} = \frac{1}{27}\Gamma$, $\Gamma_{42} = \frac{1}{54}\Gamma$, $\Omega_s = 0.75\Gamma$, $\Omega_p = 0.01\Gamma$, $\kappa_2 = \kappa_4 = \kappa_6 = \kappa$, and $\Delta = 2.15\Gamma$.

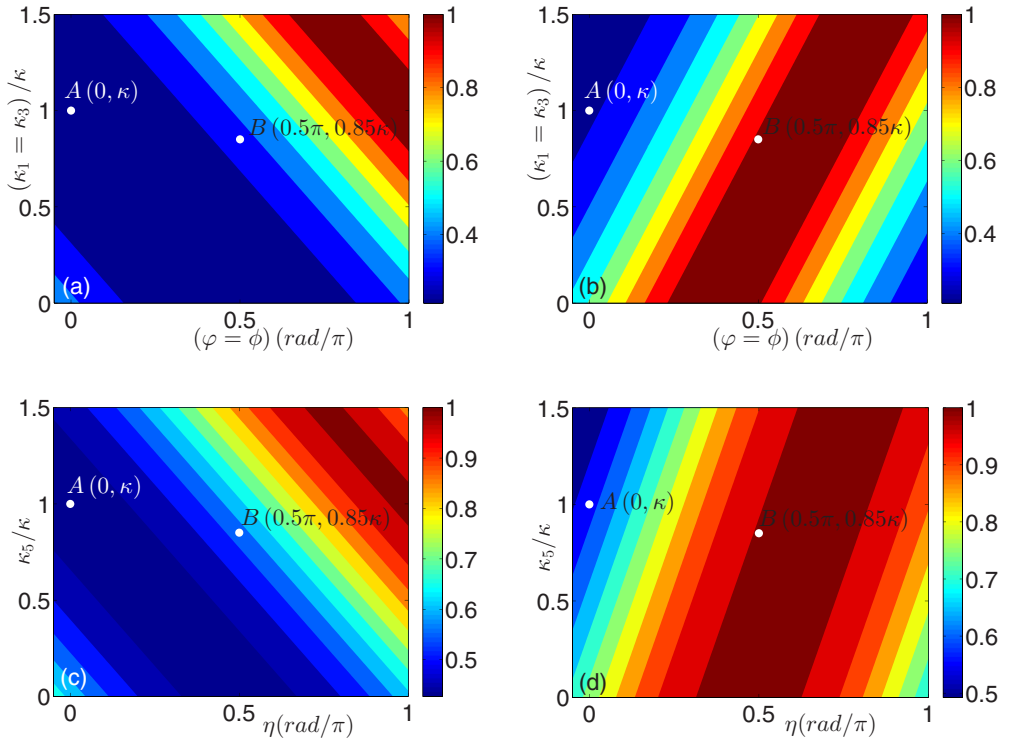

FIG. 5. The visibility V as a function of $(\varphi=\phi,\kappa_1=\kappa_3)$ for different situations with the units of the wave vectors κ_1 and κ_3 being rad/nm. (a) $(\eta,\kappa_5)=(0,\kappa)$, $(x,y,z)=(0.5,0.5,0.5)$; (b) $(\eta,\kappa_5)=(0,\kappa)$, $(x,y,z)=(-0.3,-0.3,-0.35)$. The visibility V as functions of (η,κ_5) for different situations with the units of the wave vector κ_5 being rad/nm. (c) $(\varphi=\phi,\kappa_1=\kappa_3)=(\pi/2,0.85\kappa)$, $(x,y,z)=(0.5,0.5,0.5)$; (d) $(\varphi=\phi,\kappa_1=\kappa_3)=(\pi/2,0.85\kappa)$, $(x,y,z)=(-0.3,-0.3,-0.35)$. The other values of the parameters are $\Gamma=3.6898\times10^7$ s^{-1}, $\Gamma_{32}=\frac{1}{27}\Gamma$, $\Gamma_{42}=\frac{1}{54}\Gamma$, $\Omega_s=0.75\Gamma$, $\Omega_p=0.01\Gamma$, $\kappa_2=\kappa_4=\kappa_6=\kappa$, and $\Delta=2.15\Gamma$.

Fig. 4(c), it can be found from Fig. 6(a) that two ellipsoidal shells with different sizes are situated in subspaces (x,y,z) and $(-x,-y,-z)$, respectively. As the excited population n_e is tuned to 0.385 with keeping all other parameters fixed, the atoms are mainly distributed in subspace (x,y,z), and the smaller ellipsoidal shell situated in subspace $(-x,-y,-z)$ disappears as shown in Fig. 6(b). Direct comparison in Figs. 6(a) and 6(b) implies that the probability of finding the atom at a particular position in 3D space is indeed increased by a factor of two when the excited population n_e increases from 0.355 to 0.385. More interestingly, when the excited population n_e increases to 0.415, the atoms are completely localized in subspace (x,y,z) with very small ellipsoidal structure, as shown in Fig. 6(c). In this case, the high-precision 3D atom localization is indeed achieved, and the probability of finding the atom within a cubic wavelength is significantly improved by a factor of eight compared with Refs. [41,42]. Thus, the single-position information of the atom in 3D space has been achieved in our present system.

IV. CONCLUSION

Before concluding, it should be noted that the present study focuses only on the cold atomic system, and the results of Doppler-broadening effects can be included by first rewriting the corresponding detunings, i.e., $\Delta_1=\omega_{31}-\omega_s-\Delta_{a1}=\omega_{32}-\omega_p-\Delta_{a1}$ and $\Delta_2=\omega_{41}-\omega_p-\Delta_{a2}=\omega_{42}-\omega_s-\Delta_{a2}$, with $\Delta_{a1}\sim\kappa_s,\kappa_p$ and $\Delta_{a2}\sim\kappa_p,\kappa_s$ the corresponding additional broadening effects. Based on the experimental values of the system parameters [46], one can readily check

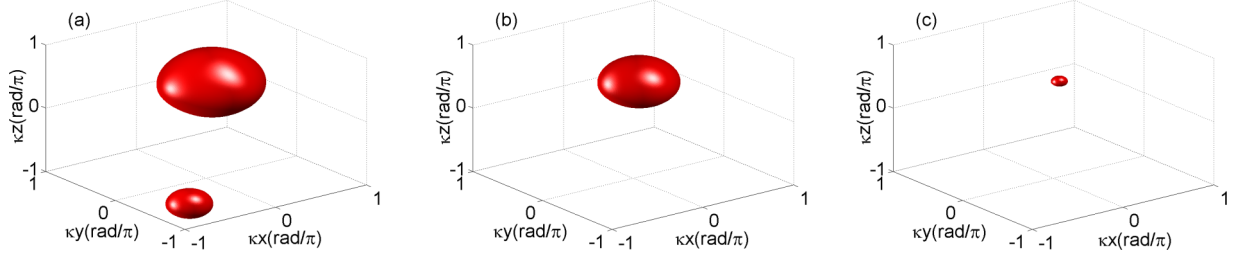

FIG. 6. The 3D conditional position probability distribution as functions of $(\kappa x,\kappa y,\kappa z)$ for different values of the excited population n_e with the units of the wave vector κ being rad/nm. (a) $n_e=0.355$; (b) $n_e=0.385$; (c) $n_e=0.415$. The other values of the parameters are $\Gamma=3.6898\times10^7 s^{-1}$, $\Gamma_{32}=\frac{1}{27}\Gamma$, $\Gamma_{42}=\frac{1}{54}\Gamma$, $\Omega_s=0.75\Gamma$, $\Omega_p=0.01\Gamma$, $\kappa_1=\kappa_3=\kappa_5=0.85\kappa$, $\kappa_2=\kappa_4=\kappa_6=\kappa$, $\varphi=\phi=\eta=\pi/2$, and $\Delta=2.15\Gamma$.

that the additional broadening has a negligible influence on the present results for the cold atomic system.

In conclusion, we analyzed in detail the behavior of 3D atom localization via phase-sensitive spatial interference in a double two-level atomic system. Due to the spatial-position-dependent atom-field interaction, 3D atom localization can be achieved by the measurement of the excited population n_e. It is clearly shown that the precision of 3D atom localization is extremely sensitive to the detuning Δ of the relevant optical fields and the phase shifts of the corresponding standing-wave fields with slightly different wavelengths. The main advantage of our proposed scheme is that we obtained single-position information of the atom with high precision in 3D space, and the probability of finding the atom in 3D space is significantly improved by a factor of eight by adjusting the excited population n_e to $n_e = 0.415$, which is originated from the phase-sensitive spatial-interference effect induced by the standing-wave fields and the probe field in the present system. Finally, it is worth noting that our proposed scheme for 3D atom localization may be useful for the high-precision measurement of the center-of-mass wave function of moving atoms and atom lithography.

ACKNOWLEDGMENTS

We would like to thank Professor Ren-Gang Wan for his encouragement and helpful discussions. The research is supported in part by National Natural Science Foundation of China under Grants No. 11374050 and No. 61372102, by Qing Lan project of Jiangsu, and by the Fundamental Research Funds for the Central Universities under Grant No. 2242012R30011 as well as by the Scientific Research Foundation of Graduate School of Southeast University No. YBJJ1522.

[1] H. Metcalf and P. Van der Straten, Phys. Rep. **244**, 203 (1994).
[2] W. D. Phillips, Rev. Mod. Phys. **70**, 721 (1998).
[3] K. S. Johnson, J. H. Thywissen, W. H. Dekker, K. K. Berggren, A. P. Chu, R. Younkin, and M. Prentiss, Science **280**, 1583 (1998).
[4] A. N. Boto, P. Kok, D. S. Abrams, S. L. Braunstein, C. P. Williams, and J. P. Dowling, Phys. Rev. Lett. **85**, 2733 (2000).
[5] G. P. Collins, Phys. Today **49**(3), 18 (1996).
[6] Y. Wu, X. X. Yang, and C. P. Sun, Phys. Rev. A **62**, 063603 (2000).
[7] Y. Wu and R. Cote, Phys. Rev. A **65**, 053603 (2002).
[8] J. Evers, S. Qamar, and M. S. Zubairy, Phys. Rev. A **75**, 053809 (2007).
[9] J. Mompart, V. Ahufinger, and G. Birkl, Phys. Rev. A **79**, 053638 (2009).
[10] M. Born and E. Wolf, *Principles of Optics* (Cambridge University Press, Cambridge, 1999).
[11] J. E. Thomas, Phys. Rev. A **42**, 5652 (1990).
[12] K. D. Stokes, C. Schnurr, J. R. Gardner, M. Marable, G. R. Welch, and J. E. Thomas, Phys. Rev. Lett. **67**, 1997 (1991).
[13] J. R. Gardner, M. L. Marable, G. R. Welch, and J. E. Thomas, Phys. Rev. Lett. **70**, 3404 (1993).
[14] P. Storey, M. Collett, and D. Walls, Phys. Rev. Lett. **68**, 472 (1992).
[15] P. Storey, M. Collett, and D. Walls, Phys. Rev. A **47**, 405 (1993).
[16] P. Storey, T. Sleator, M. Collett, and D. Walls, Phys. Rev. A **49**, 2322 (1994).
[17] S. Kunze, G. Rempe, and M. Wilkens, Europhys. Lett. **27**, 115 (1994).
[18] R. Quadt, M. Collett, and D. F. Walls, Phys. Rev. Lett. **74**, 351 (1995).
[19] S. Kunze, K. Dieckmann, and G. Rempe, Phys. Rev. Lett. **78**, 2038 (1997).
[20] F. Le Kien, G. Rempe, W. P. Schleich, and M. S. Zubairy, Phys. Rev. A **56**, 2972 (1997).
[21] S. Qamar, S. Y. Zhu, and M. S. Zubairy, Phys. Rev. A **61**, 063806 (2000).
[22] K. T. Kapale, S. Qamar, and M. S. Zubairy, Phys. Rev. A **67**, 023805 (2003).
[23] J. T. Chang, J. Evers, M. O. Scully, and M. S. Zubairy, Phys. Rev. A **73**, 031803(R) (2006).
[24] E. Paspalakis and P. L. Knight, Phys. Rev. A **63**, 065802 (2001).
[25] H. Nha, J.-H. Lee, J.-S. Chang, and K. An, Phys. Rev. A **65**, 033827 (2002).
[26] F. Ghafoor, S. Qamar, and M. S. Zubairy, Phys. Rev. A **65**, 043819 (2002).
[27] M. Sahrai, H. Tajalli, K. T. Kapale, and M. S. Zubairy, Phys. Rev. A **72**, 013820 (2005),
[28] K. T. Kapale and M. S. Zubairy, Phys. Rev. A **73**, 023813 (2006).
[29] G. S. Agarwal and K. T. Kapale, J. Phys. B: At., Mol. Opt. Phys. **39**, 3437 (2006).
[30] C. Liu, S. Gong, D. Cheng, X. Fan, and Z. Xu, Phys. Rev. A **73**, 025801 (2006).
[31] Y. Wu and X. X. Yang, Phys. Rev. Lett. **78**, 3086 (1997); J. Opt. Soc. Am. B **23**, 913 (2006); Y. Wu and L. Deng, Opt. Lett. **29**, 1144 (2004).
[32] S. Qamar, J. Evers, and M. S. Zubairy, Phys. Rev. A **79**, 043814 (2009).
[33] S. Qamar, A. Mehmood, and S. Qamar, Phys. Rev. A **79**, 033848 (2009).
[34] S. Asghar and S. Qamar, Opt. Commun. **295**, 145 (2013).
[35] V. Ivanov and Y. Rozhdestvensky, Phys. Rev. A **81**, 033809 (2010).
[36] R. G. Wan and T. Y. Zhang, Opt. Express **19**, 25823 (2011).
[37] C. L. Ding, J. H. Li, R. Yu, X. Y. Hao, and Y. Wu, Opt. Express **20**, 7870 (2012).
[38] C. L. Ding, J. H. Li, X. X. Yang, D. Zhang, and H. Xiong, Phys. Rev. A **84**, 043840 (2011).
[39] Rahmatullah and S. Qamar, Phys. Rev. A **88**, 013846 (2013).
[40] Z. H. Zhu, W. X. Yang, A. X. Chen, S. P. Liu, and R. K. Lee, J. Opt. Soc. Am. B **32**, 1070 (2015).
[41] Y. H. Qi, F. X. Zhou, T. Huang, Y. P. Niu, and S. Q. Gong, J. Mod. Opt. **59**, 1092 (2012).

[42] V. S. Ivanov, Y. V. Rozhdestvensky, and K. A. Suominen, Phys. Rev. A **90**, 063802 (2014).
[43] J. C. Delagnes and M. A. Bouchene, Phys. Rev. Lett. **98**, 053602 (2007).
[44] P. Meystre and M. Sargent III, *Elements of Quantum Optics* (Springer-Verlag, Berlin, 1999).
[45] D. M. Brink and G. R. Satchler, *Angular Momentum* (Clarendon Press, Oxford, 1993).
[46] M. E. Gehm, Ph.D. thesis, Duke University, 2003 (available online at https://www.physics.ncsu.edu/jet/theses/pdf/Gehm.pdf); Properties of ^{6}Li, p. 18, available online at http://steck.us/alkalidata
[47] C. Cohen-Tannoudji, in *Frontiers in Laser Spectroscopy*, Proceedings of the Les Houches Summer School of Theoretical Physics, Session XXVII, Les Houches, 1975, edited by R. Balian, S. Haroche, and S. Liberman (North-Holland, Amsterdam, 1977), p. 55.
[48] R. Loudon, *The Quantum Theory of Light* (Clarendon Press, Oxford, 1983).
[49] D. Polder and M. F. H. Schuurmans, Phys. Rev. A **14**, 1468 (1976).
[50] T. Wong, S. M. Tan, M. J. Collett, and D. F. Walls, Phys. Rev. A **55**, 1288 (1997).
[51] G. S. Agarwal, J. von Zanthier, C. Skornia, and H. Walther, Phys. Rev. A **65**, 053826 (2002).
[52] L. L. Jin, Y. P. Niu, and S. Q. Gong, Phys. Rev. A **83**, 023410 (2011).